Kinetic-energy distributions of ions sampled from argon plasmas in a parallel-plate, radio-frequency reference cell

J. K. Olthoff, R. J. Van Brunt, and S. B. Radovanov[a)]
National Institute of Standards and Technology,[b)] Gaithersburg, Maryland 20899

J. A. Rees and R. Surowiec
Department of Electrical Engineering and Electronics, The University of Liverpool, Liverpool L693BX, United Kingdom

(Received 1 June 1993; accepted for publication 20 September 1993)

Kinetic-energy distributions are presented for ions sampled from 13.56-MHz discharges in argon in a capacitively-coupled, parallel-plate, Gaseous Electronics Conference (GEC) radio-frequency reference cell. The cell was modified to allow sampling of ions through an orifice in the grounded electrode. Kinetic-energy distributions are presented for Ar^+, Ar^{++}, Ar_2^+, ArH^+, and several trace ions for plasma pressures ranging from 1.3 Pa, where ion-atom collisions in the plasma sheath are not important, to 33.3 Pa, where collisions are important. Applied peak-to-peak radio-frequency (rf) voltages of 50, 100, and 200 V were used, and the current and voltage waveforms at the powered electrode were measured. Dependences of the ion fluxes, mean energies, and kinetic-energy distributions on gas pressure and applied rf voltage are interpreted in terms of possible ion-collision processes. The results agree with previously measured kinetic-energy distributions of ions sampled from the side of the plasma through a grounded probe for similar discharge conditions, verifying that ion kinetics are characteristic of the plasma sheath independent of where it is formed [J. K. Olthoff, R. J. Van Brunt, and S. B. Radovanov, J. Appl. Phys. **72**, 4566 (1992)].

I. INTRODUCTION

A better understanding of the factors that control ion kinetics in radio-frequency (rf) plasmas is relevant to the application of these plasmas to the processing of materials.[1,2] In the past decade, studies of ions created by rf discharges in argon have included experimental[3–13] and theoretical[14–20] investigations of ion kinetic-energy distributions (IEDs) at the electrodes. Since the ion flux striking the electrode surfaces in argon discharges consists predominantly of Ar^+, the attention of most earlier studies has focused on this ion. However, we demonstrated[21] that a detailed investigation of the less prominent ions, such as Ar^{++}, Ar_2^+, and ArH^+, in an rf plasma can provide important information about ion formation, plasma-sheath characteristics, and the behavior of ions within the sheath.

Measured energy distributions of the minor ions in a "simple" argon plasma indicate the occurrence of processes that should be included in theoretical models. Interpretation of these energy distributions provides information about the regions of the discharge where the ions are formed and the relative importance of collisions in the sheath. Furthermore, the monitoring of ion energies and fluxes provides a sensitive probe of the microscopic conditions of the discharge. In this work these points are addressed in a detailed study of the kinetic-energy distributions for many ions sampled from argon discharges generated in the Gaseous Electronics Conference (GEC) rf Reference Cell[22] used in our earlier investigations.[21,23]

The GEC cell is a capacitively-coupled, parallel-plate rf discharge cell for which a thorough electrical characterization has been performed.[22,24] The measurement of IEDs in the present study was accomplished using a mass spectrometer with an electrostatic energy analyzer that was installed to monitor the ion flux passing through a small aperture in the grounded electrode. This work represents an extension of a previous study,[21] in which ions were sampled from the side of a GEC cell using a different type of energy analyzer-mass spectrometer system. The present experimental arrangement has the following advantages: 1) it permits better detection sensitivity; 2) it allows measurements over a greater range of pressures; 3) it does not perturb the plasma with the insertion of an ion sampling probe; 4) it represents a sampling geometry similar to that used for other ion-energy measurements;[3–8] and 5) it monitors a plasma parameter that is commonly calculated in plasma models, i.e., ion flux striking one of the parallel-plate electrodes. Compared with the method used in our earlier work,[21] the present method has the disadvantages associated with difficulties in mounting the probe in the electrode, lack of flexibility in positioning the probe, and somewhat poorer energy resolution. The present work has enabled us to test the hypothesis that ions sampled through a grounded probe around which a sheath forms will exhibit a similar energy distribution as ions sampled directly through the grounded electrode, i.e., the ion kinetics should be characteristic of the "ground" sheath, independent of where the sheath is formed.

II. EXPERIMENT

Details about the characteristics of the GEC cell used in the present work are described elsewhere.[22,24,25] This cell

[a)]Permanent address: Institute of Physics, 11000 Belgrade, Yugoslavia.
[b)]Electricity Division, Electronics and Electrical Engineering Laboratory, Technology Administration, U. S. Department of Commerce.

 0021-8979/94/75(1)/115/11/$6.00

contains two 10.2-cm-diameter aluminum parallel-plate electrodes with an interelectrode spacing of 2.54 cm, and has a configuration geometrically similar to that used in our earlier work.[21] Argon gas (99.999% purity) was supplied to the cell through a showerhead arrangement of small holes in the lower electrode. For pressures above 4 Pa, the gas is pumped out by a mechanical vacuum pump through six symmetrically placed holes in the base of the reactor. At lower pressures, the gas flow is maintained by pumping with a variable speed turbopump through one of the side ports. The argon flow rate was maintained at 1.7×10^{-2} Pa m^3/s (10 sccm).

The lower electrode is powered by a 13.56-MHz ENI rf power supply[26] coupled through a 0.1-μF blocking capacitor and an isolating rf filter.[27] Voltage and current waveforms were measured at the base of the powered electrode using a digital oscilloscope. Peak-to-peak amplitudes of the measured rf voltage waveform (V_{rf}) specifically refer to the applied voltage as in previously reported GEC cell measurements.[22] The amplitudes and phases of the Fourier components reported here apply to the current and voltage waveforms at the surface of the powered electrode as calculated using an equivalent circuit model of the GEC cell.[22,24] These values are referred to as the plasma current and plasma voltage.

To sample ions through an aperture in the grounded upper electrode, it was necessary to switch the showerhead electrode assembly, normally grounded in the upper position, to the lower position, and to redesign the upper-electrode assembly to accommodate the ion-energy measurement system as shown in Fig. 1. The ceramic insulator on which the electrode is normally mounted was replaced with a stainless-steel tube that supported an aluminum electrode containing a 0.1-mm sampling orifice. No ground shield is required for this electrode since the entire support assembly is made of stainless steel and is grounded by way of the mounting bolts. Because of the low-power plasmas used (<4 W), water cooling of the electrodes was deemed unnecessary for the present work. Although the modifications to the GEC cell slightly changed its inherent capacitance and inductance, the resulting changes in calculated plasma voltage and current are within the uncertainties previously determined for other GEC rf Reference Cells.[22]

Ion kinetic-energy distributions were measured using a Hiden EQP Plasma probe[26] which consists of an electrostatic ion-energy analyzer (ESA) coupled to a quadrupole mass spectrometer (QMS) configured as shown in Fig. 1. Positive ions are accelerated from the glow region of the plasma toward the surface of the anode by the electric fields present in the plasma sheath at the grounded electrode. A small fraction of these ions enter the aperture located at the center of the grounded electrode where they are accelerated into the drift region that precedes the ESA by a constant applied field between the electrode and the extractor. Ion kinetic-energy distributions are measured by setting the quadrupole to a particular mass-to-charge ratio and then scanning the energy of the ions allowed to pass through the electrostatic energy analyzer. The voltages on the ion optics are ramped such that all ions pass through

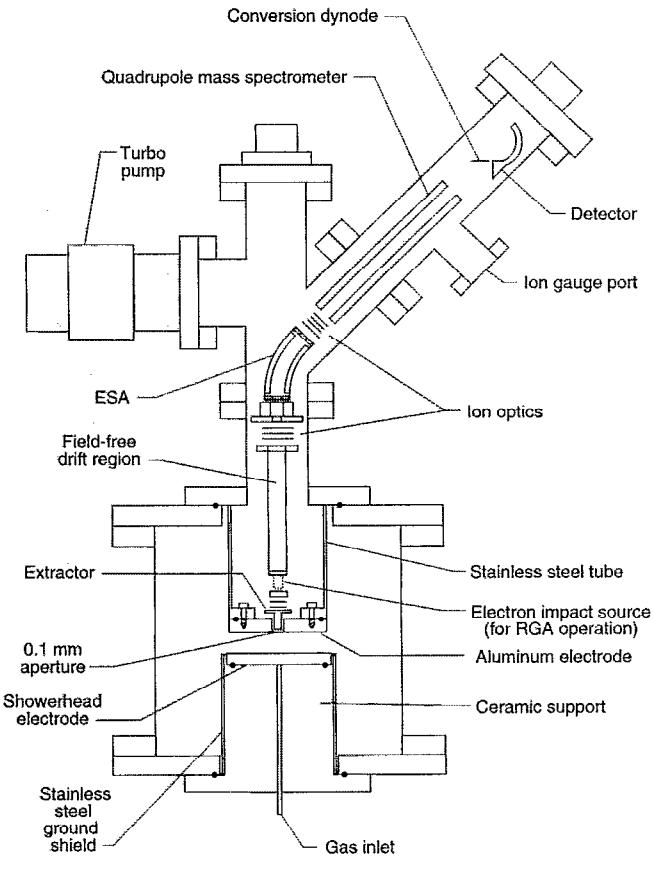

FIG. 1. Schematic diagram of the mass spectrometer with energy analyzer mounted on the top of the GEC rf Reference Cell. The ESA is a 45° electrostatic ion-energy analyzer. The electron-impact ion source can be used to ionize neutrals sampled from the plasma region, but is not used when sampling ions directly from the discharge. For simplicity, the side ports of the GEC cell are not shown.

the ESA to the quadrupole with the same energies, independent of their initial kinetic energy. The energy resolution of the ESA was approximately 1.5 eV (full width at half maximum) for the operating conditions used here. Adjustments to the energy scale required for the previous off-axis ion-energy measurements[21] were deemed unnecessary for the present work. The uncertainty in the energy scale is determined by uncertainties in plate voltages and variations in surface potentials, and is approximately ±1 eV.

All data for a particular ion were obtained with the same analyzer settings and scan rates to allow comparison of signal intensities for the *same* ion under different plasma conditions. However, conversion dynode voltages and scan rates were adjusted for each ion in order to provide adequate ion intensities without saturating the electron multiplier. Thus meaningful determinations of relative ion fluxes for *different* ions can not be derived from the data presented here.

Differential pumping of the vacuum chambers maintains pressures below 10^{-4} Pa inside the ESA-QMS vacuum housing for gas pressures inside the GEC cell of up to 35 Pa. The fraction of ions that experience a collision after passing through the orifice and before reaching the detec-

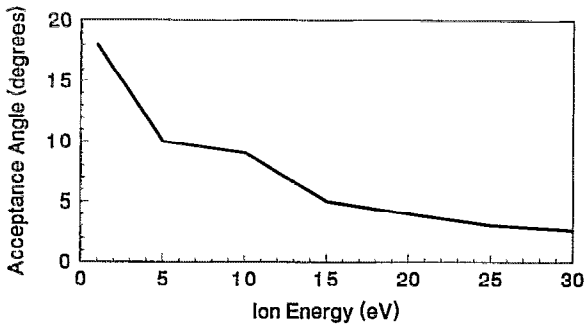

FIG. 2. Plot of acceptance angle of the ion energy analyzer-mass spectrometer system as a function of initial ion kinetic energy. The acceptance angle is defined as the largest trajectory angle that an ion with a certain kinetic energy may have, as it exits the sampling orifice, that will still allow the ion to be transmitted through the ESA. The acceptance angle is defined with respect to the normal to the back of the electrode surface.

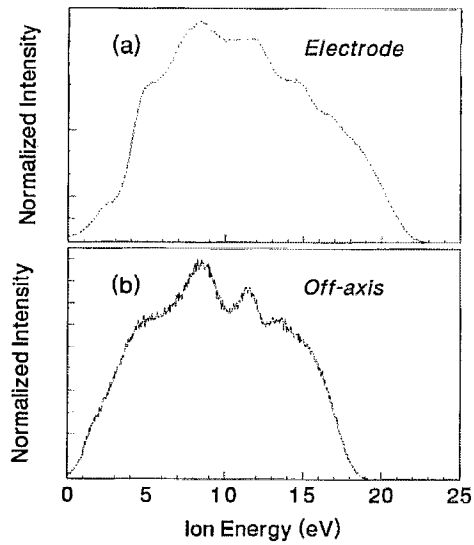

FIG. 3. Kinetic-energy distributions for Ar^+ ions sampled from an argon plasma in a GEC rf Reference Cell with $V_{rf}=200$ V and a gas pressure of 13.3 Pa. "ELECTRODE" – Ions are sampled through the grounded electrode by the apparatus described in this report. "OFF-AXIS" – Ions are sampled through a grounded sampling cone positioned on the side of the discharge at a point mid-way between the electrodes near the inner edge of the ground shield. Details of this sampling geometry and the mass spectrometer-ion energy analyzer system used to obtain these data are available elsewhere (see Ref. 21).

tor can be estimated[7,28] for the conditions used here. It is estimated that in the extreme case of low energy ions (~1 eV) and high plasma pressures (33.3 Pa), a maximum of 28% of the ions sampled through the orifice will experience a collision before detection. This decreases to 20% for 20-eV ions. For pressures of 13.3 and 1.3 Pa, the percentage of 1-eV ions experiencing a collision in the analyzer is approximately 12% and 1%, respectively. Thus only at higher pressures does one anticipate significant distortions of the IEDs by ion-atom collisions downstream of the sampling orifice.

Another source of IED distortion is the energy-dependent acceptance angle of the ion energy analyzer-mass spectrometer system. Calculations of ion trajectories were performed using the SIMION software package[29] to determine acceptance angles for the operating conditions used here. It was necessary to carry out the calculations in two parts. The trajectories of ions from the back of the grounded electrode to the entrance of the energy analyzer were first calculated. The resulting ion acceptance angles are presented in Fig. 2 as a function of initial ion kinetic energy at the sampling orifice. The ion acceptance angle is defined here as the maximum angle, with respect to the axis of the drift region, that an ion may have as it exits the orifice such that it is transmitted through the ion-energy analyzer. The acceptance angle was found to be 18° for 1-eV ions, decreasing to approximately 3° for 30-eV ions. The results were nearly independent of mass for ions with a mass-to-charge ratio between 20 and 80 u.

In the second part, trajectories were calculated for ions starting in the plasma sheath to determine the ion angular distributions at the exit of the sampling orifice. This calculation takes into account the focussing effects of the fields present at the orifice. It was necessary, for conditions under which the ions suffered collisions in crossing the sheath, to distinguish between elastic collisions and charge-exchange collisions. The charge-exchange process was assumed to yield ions with approximately thermal kinetic energies. Of course, in the limit of very low-energy collisions, the distinction between charge-transfer and elastic collisions becomes unclear. The calculations showed that, for the case of elastic collisions, the acceptance angle of the orifice (defined here as the maximum angle, with respect to the normal to the surface of the grounded electrode, that an ion may have as it approaches the orifice such that it subsequently passes through the orifice into analyzer region) for ions released at different points in the sheath was largely independent of the ion energy for values ranging from 1 to 30 eV, but varied by a factor of four over the width of a typical sheath.[30] For ions formed with thermal energies the orifice acceptance angle varied for typical plasma conditions from about 40° to 25° as a function of the position in the sheath at which the charge-exchange collision was assumed to have occurred.

At all the experimental conditions modeled, ions that are successfully sampled from the plasma (i.e., accepted by the sampling orifice) subsequently enter the drift region and the energy analyzer at angles which are within the acceptance angles shown in Fig. 2. In other words, this analysis suggests that the existence of any energy discrimination effects are not predominantly due to ion transit through the drift region and energy analyzer.

III. RESULTS

A. Comparison of "off-axis" and "through-the-electrode" sampling

A representative kinetic-energy distribution for Ar^+ ions sampled from a 13.3-Pa argon plasma with $V_{rf}=$ 200 V is shown in Fig. 3(a) as measured through the grounded electrode by the present apparatus. The energy distribution displays typical structure for the case where collisions are important.[7–9] For comparison, an IED for

Ar^+, as measured previously[21] from the side of the parallel-plate discharge, is shown in Fig. 3(b). The shapes of the distributions are remarkably similar with the corresponding energies of the secondary maxima in each distribution agreeing to within an electron volt. The similarities indicate that the IEDs are characteristic of the sheath in front of a grounded surface, independent of where the surface is located. In general, the IEDs for all observed ions exhibit features consistent with those measured with the off-axis probe in cases where a sheath is known to be formed at the probe surface.

The signal-to-noise ratio in Fig. 3(a) is indicative of the higher sensitivity of the present instrument, while the differences in the widths of the secondary peaks are the result of differences in energy resolution [1.5 eV in Fig. 3(a), and 0.5 eV in Fig. 3(b)]. The most significant difference between the IEDs is that the maximum kinetic energy observed in Fig. 3(b) is nearly 4 eV less than for the distribution in Fig. 3(a). A number of factors could account for this difference, such as 1) differing energy resolutions, 2) differences in acceptance angles of the instruments, and 3) different materials in which the sampling orifices are located (aluminum versus stainless steel). Differing materials could be especially important because they may have different surface-charging characteristics and secondary emission coefficients when exposed to the plasma. It is perhaps worth noting that the observed difference in the maximum kinetic energies is of the same magnitude as the energy correction required to obtain the previous data.[21]

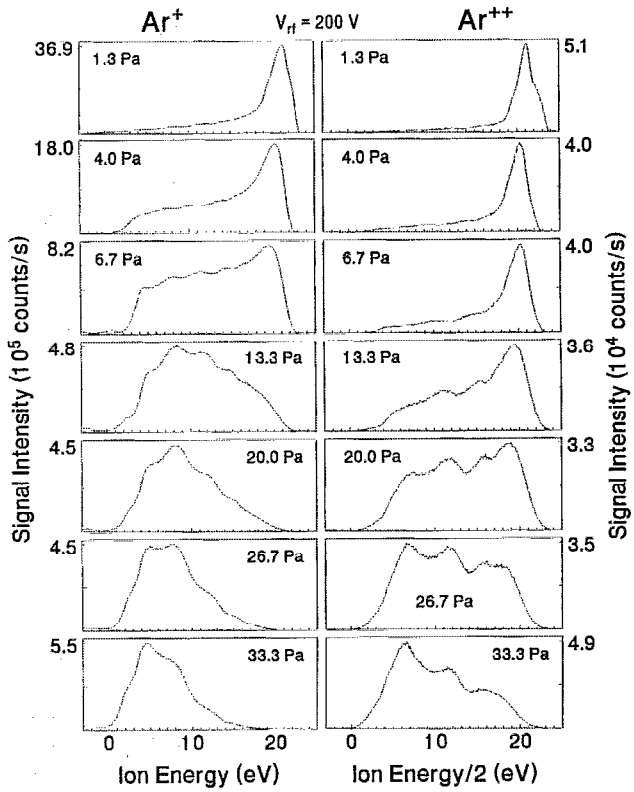

FIG. 4. Measured kinetic-energy distributions for Ar^+ and Ar^{++} sampled from argon plasmas at the indicated pressures and with $V_{rf}=200$ V. The energy scale for the Ar^{++} IEDs has been divided by 2 due to the double charge on the ion. The baseline of the IEDs in Figs. 4–9 corresponds to 0 counts/s.

B. Ar^+ and Ar^{++}

Shown in Fig. 4 are the kinetic-energy distributions for Ar^+ and Ar^{++} ions sampled from argon discharges as a function of pressure for $V_{rf}=200$ V. The kinetic-energy scale for the Ar^{++} IEDs is divided by 2 due to the double charge on the ion. This makes it easier to compare the Ar^{++} IEDs with those of other ions, and to compare the ion energies with the plasma potential.

At 1.3 Pa, both ionic species possess narrow IEDs peaked near 21 eV (corresponding approximately to the time-averaged sheath potential) with low-energy tails extending down toward 0 eV. The shape of the Ar^+ IED is in agreement with the Monte-Carlo calculations of Liu *et al.*,[7] but does not exhibit the low-energy peak that they observed experimentally. The fact that the IEDs are peaked at higher energies is consistent with the expectation that the majority of ions are formed by electron impact in the bulk plasma, near the sheath-plasma interface, where the density of energetic electrons is highest.[31] Ions that experience energy loss by collisions contribute to the low-energy portion of the IEDs. The shoulder observed on the high-energy side of the Ar^{++} peak results from the effect of the rf modulation of the sheath potential.[19] This feature is not observed for Ar^+ due to the larger mass-to-charge ratio of this ion, resulting in a longer transit time across the sheath.

The IEDs for both Ar^+ and Ar^{++} exhibit broadening, and the mean energies shift toward lower energies, as the pressure inside the cell increases, in agreement with other ion kinetic-energy measurements and calculations.[5–10,12] The secondary maxima in the Ar^+ and Ar^{++} distributions are believed to result from thermal ion formation in the sheath by charge transfer and by electron-impact ionization, respectively. It is possible that there are also small contributions to Ar^+ formation by electron collisions in the sheath. In addition, at higher pressures, both ions will lose significant energy by elastic momentum-transfer collisions.[20] At the highest pressure of 33.3 Pa, there are relatively insignificant numbers of Ar^+ or Ar^{++} ions appearing with kinetic energies corresponding to the maximum allowed by the time-averaged sheath potential.

The IEDs for Ar^{++} consistently exhibit at least one fewer secondary maximum than the IEDs for Ar^+. This is because the number of secondary maxima in the IEDs decreases with the ion transit time across the sheath.[9] Because of their higher charge, Ar^{++} ions are accelerated more and spend less time in the sheath.

As can be seen in Fig. 5, the same pressure effects for the IEDs of Ar^+ and Ar^{++} are observed when $V_{rf}=100$ V, except that the relative magnitudes of the secondary maxima are smaller and the influence of collisions becomes more pronounced at all pressures. For lower rf voltages, significant ion signals can be detected at "negative energies" for pressures exceeding 13 Pa. This signal can be

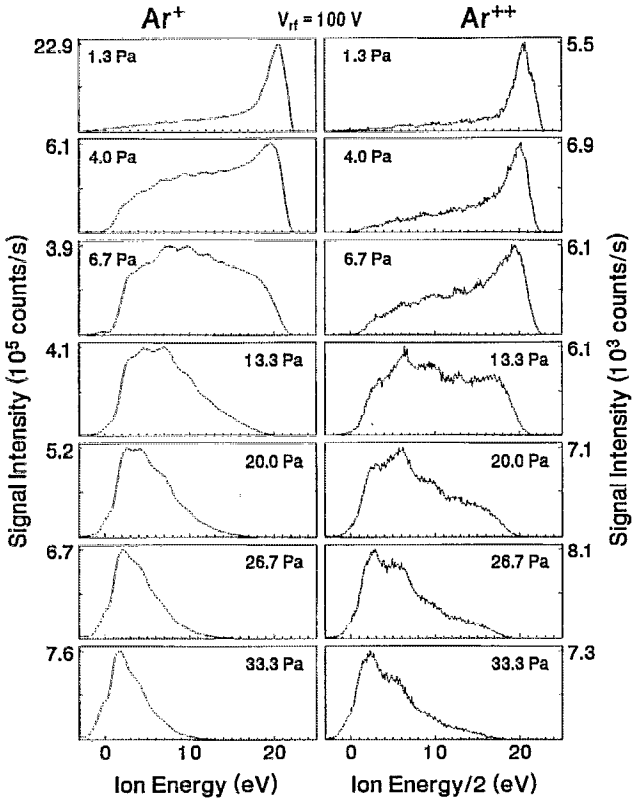

FIG. 5. Measured kinetic-energy distributions for Ar^+ and Ar^{++} sampled from argon plasmas at the indicated pressures and with $V_{rf}=100$ V. The energy scale for the Ar^{++} IEDs has been divided by 2 due to the double charge on the ion.

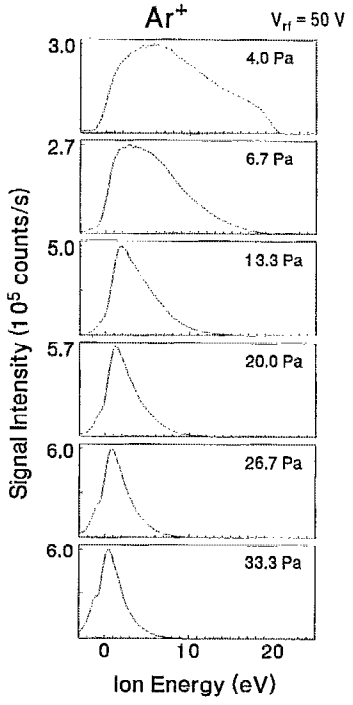

FIG. 6. Measured kinetic-energy distributions for Ar^+ sampled from argon plasmas at the indicated pressures and with $V_{rf}=50$ V. The discharge could not be sustained for pressures below about 2.0 Pa, and no measurable Ar^{++} signal was present at this rf voltage at any pressure.

due to a combination of the finite energy resolution of the ESA, the kinetic energy lost by ions in momentum-transfer collisions that occur after passing through the orifice, and the possible presence of contact potentials. The negative energy signal for Ar^+ is more pronounced because these ions can be created at thermal energies by charge-exchange collisions within the extraction field region, and would therefore not acquire sufficient energy from this field to appear at or above zero energy in the IED. The larger negative energy signals observed for low-voltage, high-pressure conditions are in accordance with calculations[7,28] indicating that the number of ion-molecule collisions occurring downstream of the orifice are greatest for low-energy ions being sampled from high-pressure plasmas.

At $V_{rf}=50$ V, it was not possible to maintain a discharge for pressures below about 2 Pa, and there was no measurable ion signal for Ar^{++} at any pressure. Also, the results in Fig. 6 show no fine structure in the Ar^+ distributions at this voltage. Moreover, at 50 V, the Ar^+ IEDs at all pressures are peaked at energies significantly below the maximum allowed by the time-averaged sheath potential, and are nearly independent of pressure above approximately 20 Pa.

C. Ar_2^+ and ArH^+

In rf discharges, Ar_2^+ is thought to be formed primarily by low-energy, three-body collisions[32,33] in the bulk plasma. It is speculated that ArH^+ is also formed primarily in the bulk plasma by ion-molecule reactions directly or indirectly involving impurities present in the discharge cell. The subsequent interactions of Ar_2^+ and ArH^+ with neutral argon, when these ions are accelerated across the sheath, are not well determined,[34,35] but the IEDs of these ions in rf discharges appear to be relatively less affected by collisions in the sheath region due primarily to an absence of charge-exchange interactions.[3-5] This is particularly evident for Ar_2^+ in Fig. 7 where the IEDs for Ar_2^+ and ArH^+ are presented for a range of argon plasma pressures and $V_{rf}=200$ V. The Ar_2^+ IEDs are free of secondary structure at all pressures considered here, indicating insignificant Ar_2^+ ion formation in the sheath. At 1.3 Pa, the effect of ion-atom collisions inside the sheath are evident only as a minor tail on the low-energy side of the distribution. The intensity of the low-energy portion of the Ar_2^+ IED increases with increasing pressure, and results in a lowering of the average ion energy. However, even at 33.3 Pa the IED is peaked near 20 eV, indicating that a majority of the detected ions have kinetic energies determined primarily by the average plasma potential.

Similar behavior is exhibited in the IEDs for ArH^+ shown in Fig. 7, except that the appearance of a significant low-energy tail occurs at lower pressures. Above 13.3 Pa, secondary structure is observed indicating possible formation of low-energy ArH^+ ions in the sheath. The increased broadening of the IEDs of ArH^+ with increasing pressure was observed previously by Greene *et al.*,[5] but their signal-

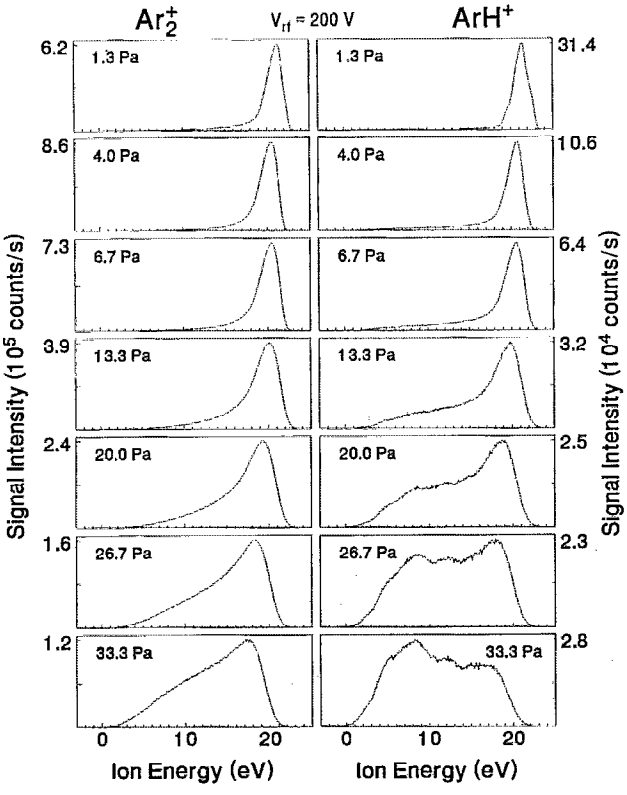

FIG. 7. Measured kinetic-energy distributions for Ar_2^+ and ArH^+ sampled from argon plasmas at the indicated pressures and with V_{rf}=200 V.

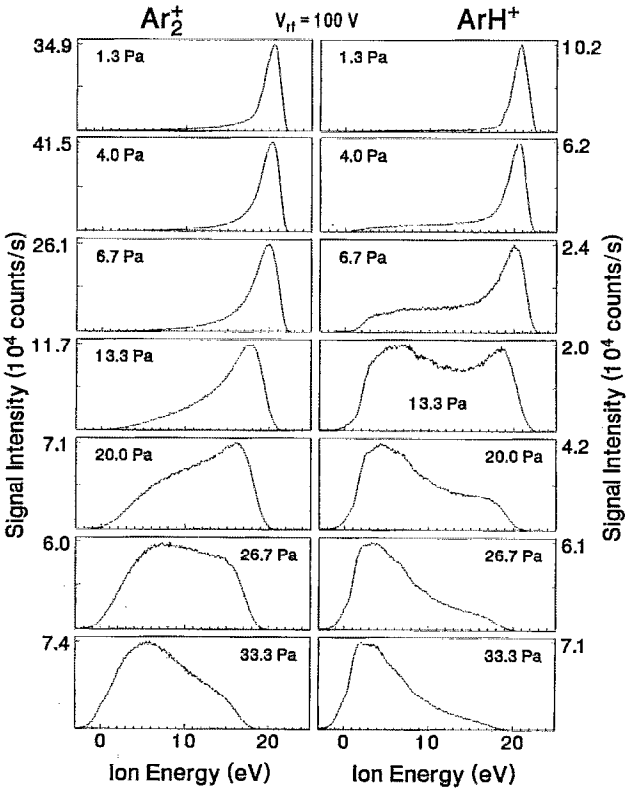

FIG. 8. Measured kinetic-energy distributions for Ar_2^+ and ArH^+ sampled from argon plasmas at the indicated pressures and with V_{rf}=100 V.

to-noise ratio was inadequate to observe the secondary structure seen here.

Figures 8 and 9 show the ion kinetic-energy distributions for Ar_2^+ and ArH^+ for applied rf voltages of 100 and 50 V, respectively. As for Ar^+ and Ar^{++}, the distributions shift toward lower energies as the pressures increase, and as V_{rf} decreases. At V_{rf}=50 V, the distributions are peaked at low energies (near thermal energy) for the highest pressures, and only at the lowest pressure plasmas do the IEDs exhibit a significant number of ions with energies corresponding to the average sheath potential. Like Ar^+, the IEDs Ar_2^+ and ArH^+ are nearly independent of pressure above 20 Pa.

D. Minor ions

Mass spectrometry has been utilized on many different rf plasma experiments to monitor the gas-phase constituents present in the discharge and to perform as an endpoint detector in etching processes.[36] In many cases, the mass spectra obtained from etching systems are sufficiently complex that a complete understanding of the chemical processes occurring in the system that yield these mass spectra is not possible.[37] The analyzer used here is equipped with an electron-impact ionizer that enables it to be used as a residual gas analyzer (RGA), similar to instruments frequently used on etching reactors. Shown in Fig. 10(a) is a mass spectrum obtained by running the plasma probe as a RGA while a 13.3-Pa argon discharge

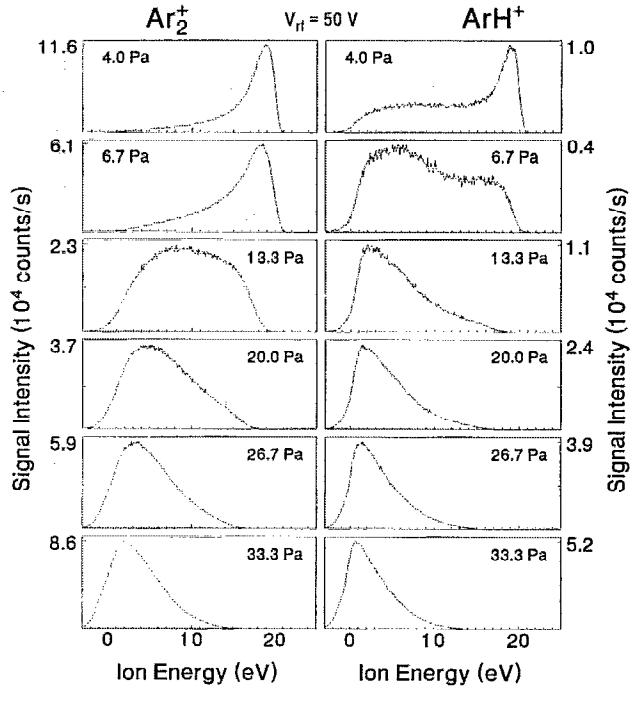

FIG. 9. Measured kinetic-energy distributions for Ar_2^+ and ArH^+ sampled from argon plasmas at the indicated pressures and with V_{rf}=50 V. The discharge could not be sustained for pressures below about 2.0 Pa.

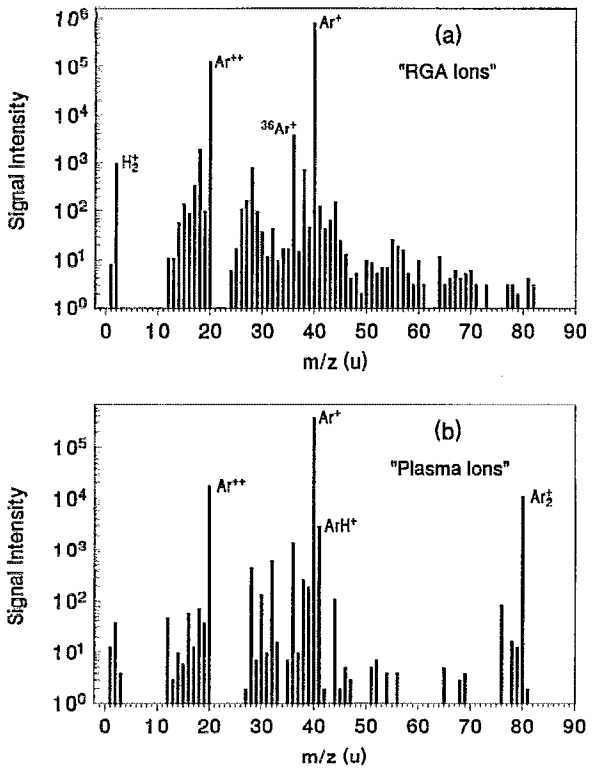

FIG. 10. (a) Residual gas analysis mass spectrum of neutral gas sampled from an argon plasma with $V_{rf}=200$ V and a gas pressure of 13.3 Pa. (b) Mass spectrum of ions formed in the same argon plasma and sampled through the orifice in the grounded electrode. The ESA was set to sample ions with kinetic energies of 19 eV.

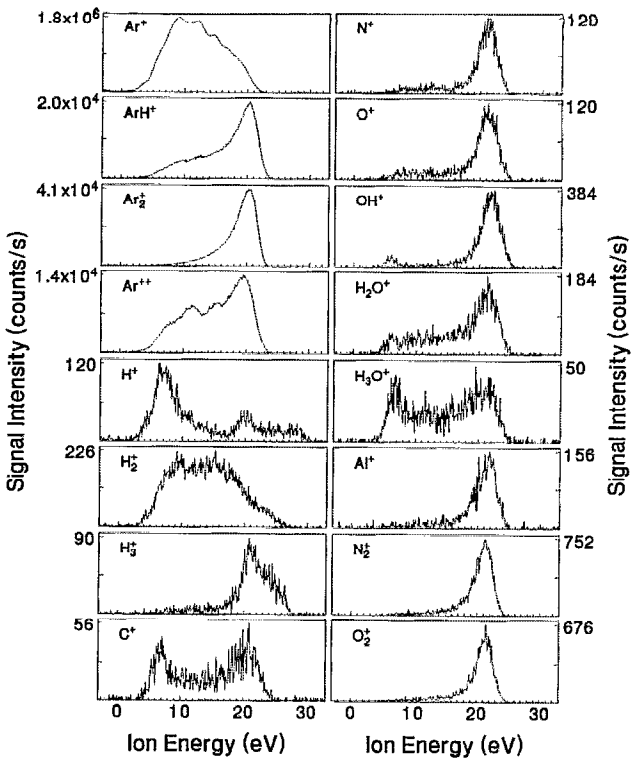

FIG. 11. Ion kinetic-energy distributions of several ions created in an argon plasma with $V_{rf}=200$ V and a gas pressure of 13.3 Pa. The labels represent the most probable ion identification for the signal corresponding to the measured mass-to-charge ratio. The baseline of the IEDs correspond to 0 counts/s. The energy scale of the IED for Ar^{++} has been divided by 2 (due to the double charge on the ion) in order to facilitate comparison with the IEDs of the other ions presented in the figure.

with $V_{rf}=200$ V was present in the GEC cell. Under these operating conditions, neutral atoms and molecules passing through the sampling orifice in the electrode are ionized by 70-eV electron impact inside the ion source preceding the ion energy analyzer (shown in Fig. 1). The two main peaks in the RGA mass spectrum are the ions that are formed directly by ionization of the argon gas. However, besides ions related to the argon feed gas, the spectrum shows a multitude of peaks that result from gas-phase impurities. The importance of these species to the chemistry of the discharge is obscured by the RGA background signal that is inherent to the analyzer vacuum system. Background pressures were less than 5×10^{-6} Pa in both the GEC cell and the plasma probe vacuum chamber prior to starting the flow of argon feed gas.

Figure 10(b) shows the corresponding mass spectrum of ions produced in the discharge that were extracted through the orifice in the grounded electrode. In obtaining this spectrum, the ESA was set to pass ions with a kinetic energy of 19 eV. This mass spectrum is less complex than the RGA spectrum since only ions formed in the discharge are detected. As expected, the four argon-related ions discussed in the previous sections dominate. All other ions have intensities nearly three orders of magnitude below the recorded intensity of Ar^+. The relative intensities of the ions in the discharge mass spectrum [Fig. 10(b)] are sensitive to conditions in the cell, such as electrode surface conditions, over which one has little or no control.

The minor ions observed in both the discharge and RGA spectra are derived from such sources as atmospheric impurities, residual water vapor, surface sputtering, and pump-oil vapor. Recent results[38,39] indicate that relatively minor changes in the level of some impurities, such as oxygen, are correlated with significant and reproducible changes in the shapes and intensities of IEDs, and with the measured plasma voltage and current waveforms.

It is important to note that the relative signal intensities shown in Fig. 10(b) do not correspond to the contribution of individual ions to the total ion flux striking the grounded electrode. The data in Fig. 10(b) only provide a measure of the relative intensity and identity of ions in the sheath with kinetic energies of approximately 19 eV. This kinetic energy was selected because most of the ions present in the plasma exhibited measurable signal at this energy. A determination of the relative contributions of ions to the total flux requires an integration over all kinetic energies.

The kinetic-energy distributions for several of the plasma ions seen in Fig. 10(b) are shown in Fig. 11. All IEDs *in this figure* were obtained under the same operating conditions so that comparisons of relative ion intensities can be made to within the uncertainties of mass discrimination effects inherent to the mass spectrometer. No at-

tempt was made to determine the magnitude of mass discrimination effects in this work. However, for a typical quadrupole mass spectrometer, variations in detection efficiency are expected to be less than a factor of two over the mass range considered. The ion labels in the figure represent the most probable identification of the signals at the corresponding mass-to-charge ratios. The Al^+ ions are undoubtedly formed by the sputtering of material from the surface of the electrodes, while the C^+ ions could come from sputtering of the stainless steel surfaces or from ionization of gas contaminants such as residual pump oil vapor or CO_2. Other ions, such as H^+, H_3O^+, O^+, and N^+ can be formed from residual water or atmospheric gases, such as nitrogen and oxygen.

The H^+ ion clearly shows the saddle structure at higher energies due to rf modulation of the sheath potential, which is expected because of its low mass.[19] It also shows a low-energy peak indicating the formation of some H^+ ions in the sheath. The H_2^+, C^+, H_2O^+, and H_3O^+ ions also exhibit a low-energy contribution in their IEDs, indicating some ion formation or significant collisional processes occurring in the sheath. The remainder of the ions are apparently formed in the bulk of the discharge and are accelerated across the sheath with little or no interaction with the argon background gas.

E. Current and voltage measurements

As discussed in the Experiment section, the voltage and current waveforms were measured near the base of the powered electrode for all plasma conditions used here. Utilizing an equivalent circuit model[22,24] of the GEC rf Reference Cell and the accompanying external circuitry, magnitudes and phases of the Fourier components of the voltage and current waveforms at the surface of the powered electrode were calculated. These values are representative of the current and voltage across the plasma.

The amplitudes of the first (fundamental) Fourier components of the plasma voltage and current waveforms, their relative phases, and the magnitudes of the dc self-bias potential and power dissipated in the plasma are presented in Table I. These values are provided in order to characterize the rf discharge and to allow for comparison of the IEDs presented here with model calculations and with IEDs measured on other rf discharge systems. The higher-order components of the voltage and current waveforms are not included here because they are small, and because they have been shown to be highly dependent upon external rf circuitry and therefore cannot be compared easily among different cells.[22,27] It should also be noted that the data shown in Table I cannot be compared with the electrical parameters reported in our earlier work (Table II of Ref. 21) which corresponded to uncorrected raw data.

TABLE I. Amplitudes (half of peak-to-peak) of the fundamental components of the plasma voltage (V_1) and current (I_1) waveforms, their relative phases (ϕ_1), the dc self-bias potential (V_b), and the power dissipated in the plasma as a function of the applied peak-to-peak rf voltage (V_{rf}) and gas pressure. These values are calculated from the voltage and current waveforms measured near the base of the powered electrode using the an equivalent circuit model of the cell. The phase of I_1 is arbitrarily set to zero.

V_{rf} (V)	Pressure (Pa)	V_1 (V)	I_1 (mA)	ϕ_1 (°)	V_b (V)	Power (W)
200	1.3	117.2	84	−68.1	−101.5	1.84
	4.0	116.4	116	−73.3	−99.2	1.94
	6.7	116.3	140	−74.9	−96.8	2.11
	13.3	118.0	189	−76.6	−95.5	2.58
	20.0	117.7	227	−77.4	−93.8	2.92
	26.7	119.7	265	−77.8	−94.3	3.34
	33.3	118.7	293	−78.0	−92.5	3.62
100	1.3	59.8	46	−62.1	−44.4	0.64
	4.0	60.5	66	−68.8	−42.8	0.72
	6.7	60.8	80	−70.7	−40.9	0.80
	13.3	61.3	105	−72.3	−39.5	0.98
	20.0	60.5	123	−73.0	−38.0	1.09
	26.7	61.6	142	−73.6	−38.2	1.23
	33.3	61.1	154	−73.8	−37.3	1.32
50	4.0	30.3	30	−56.5	−14.1	0.25
	6.7	30.1	36	−58.7	−11.6	0.28
	13.3	29.7	43	−60.0	−9.9	0.32
	20.0	29.5	50	−61.0	−9.7	0.35
	26.7	30.3	58	−62.9	−10.6	0.40
	33.3	30.2	62	−63.5	−10.2	0.42

IV. DISCUSSION AND CONCLUSIONS

The characteristics of the IEDs for Ar^+, Ar_2^+, Ar^{++}, and ArH^+ are consistent with results from our earlier measurements performed "off-axis" with a different ion energy analyzer-mass spectrometer system.[21] The agreement observed in Fig. 3 increases the confidence with which one views the IEDs presented here and in Ref. 21. It also confirms the appropriateness of sampling ions from the plasma through a separately grounded sampling element (as done in Refs. 10 and 21).

Analysis of changes in the IEDs as the plasma pressure is varied from nearly collisionless to highly collisional conditions provides information about the sheath conditions, and about ion formation processes and ion-molecule interactions affecting the ion flux through the sheath. Under collisionless conditions, the maximum energy that an ion can gain is nearly equal to the maximum sheath potential, which for a grounded electrode is equal to the instantaneous maximum plasma potential. However, at these pressures, an ion typically takes many rf cycles to traverse the sheath, so the ion kinetic energy is a measure of the time-averaged plasma potential relative to ground. As the pressure increases, a greater number of collisions occur in the sheath that cause a reduction of the ion kinetic energy. These ions reach the surface of the grounded electrode with only a fraction of the maximum allowed kinetic energy determined by continuous acceleration across the entire sheath. The degree to which the energies of different ions are decreased by collisions is dependent upon the collisional processes that affect each ion.

Monte Carlo calculations show that a reduction of the mean Ar^+ ion energy due to charge-exchange and elastic scattering collisions increases with increasing pressure.[20] Charge-exchange collisions are responsible for the second-

ary maxima in the IEDs for Ar^+ because they allow formation of ions with close to zero energy in the time-varying field of the sheath. Although no significant charge-exchange can occur for Ar^{++} colliding with argon, secondary maxima are still observed due to the formation of thermal ("zero" energy) ions in the sheath by electron-impact ionization. The IEDs for Ar^{++} do not exhibit as large a shift toward lower energies with increasing pressure as that observed for Ar^+. This is expected if detected Ar^{++} ions experience no charge-exchange collisions and therefore are formed with greatest probability by high-energy electrons that are most abundant near the sheath-plasma boundary.

The IEDs for Ar_2^+ are essentially featureless, indicative of ions formed predominately in the bulk of the plasma, and are more sharply peaked at high energy than other ions, due to less loss of energy by collisions. The IEDs for ArH^+ are quite similar to those of Ar_2^+, except that a low-energy tail, replete with secondary structure, appears in the ArH^+ IEDs at elevated pressures. It is known that the reaction

$$Ar^+ + H_2 \rightarrow ArH^+ + H \tag{1}$$

is very fast ($k = 1.7 \times 10^{-9}$ cm^3/s), proceeding at nearly the collision rate for thermal energies.[35,40] The RGA mass spectrum in Fig. 10(a) indicates a significant concentration of gas-phase H_2 in the discharge cell when the discharge is present. The origin of the hydrogen gas is not known, but its presence can explain the formation of ArH^+ in light of the above reaction. The existence of secondary maxima in the ArH^+ IEDs at elevated pressures (Fig. 7) indicates that a significant number of ArH^+ ions are created within the sheath region with thermal kinetic energy. Interactions of H_2 with thermal Ar^+ ions formed by charge transfer may produce the observed structure. Slower ion-atom reactions, such as

$$H_2^+ + Ar \rightarrow ArH^+ + H \tag{2}$$

$$ArH^+ + Ar \rightarrow Ar + ArH^+ \tag{3}$$

can also contribute to the production of ArH^+.[35] Additionally, formation of ArH^+ by interactions of Ar^+ with water molecules is also a possibility, but little is known about these reactions.

For $V_{rf} = 200$ V, the maximum kinetic energies observed for Ar_2^+ and ArH^+ are nearly constant at all pressures, even though significant changes in the self-bias potentials are observed. This implies that the time-averaged potential across the sheath at the grounded electrode is essentially unaffected by changes in the gas pressure, i.e., changes in the self-bias mainly affect the potential across the sheath in front of the powered electrode. The observation that the number and corresponding energies of the secondary maxima in the IEDs for Ar^+ and Ar^{++} also remain constant as a function of pressure further supports this conclusion. Wild and Koidl,[9] however, observed a significant shift in secondary structure as the pressure was varied. This difference is due to the much larger ratio of the powered-to-grounded electrode areas of the rf cell used by Wilde and Koidl as compared to the electrode geometry of the GEC cell. The rf reactor of Wild and Koidl[9] produces a sheath at the grounded electrode that exhibits a much larger potential drop than the sheath near the powered electrode, which is opposite of that for a GEC cell.

The applied voltage dependence of the ion kinetic-energy distributions for the various ions can be determined by comparing the IEDs in Figs. 4–6 for Ar^+ and Ar^{++}, and Figs. 7–9 for Ar_2^+ and ArH^+. For ions exhibiting multipeaked structure in their IEDs, a decrease in V_{rf} causes the relative amplitudes of the secondary maxima to decrease. This is in agreement with the experimental and calculated IEDs of Liu *et al.*,[7] and with previous measurements made in this laboratory.[21] It is also apparent that the shift toward lower energies with increasing pressure is more dramatic for plasmas with lower applied voltages, again indicating an increasingly important role played by momentum transfer in elastic collisions.

For constant pressures below 13.3 Pa, the time-averaged sheath potential, as determined by the kinetic energy corresponding to the peak in the IEDs for Ar_2^+, remains essentially unchanged for applied rf voltages ranging from 50 to 200 V. This agrees with voltage measurements for argon plasmas in the GEC cell indicating that changes in V_{rf} are observed primarily across the powered sheath,[41] and optical emission measurements indicating that the emission in the region near the ground sheath does not change significantly with applied voltage.[42] This type of rf plasma behavior has been shown to be indicative of significant secondary-electron emission from surfaces exposed to the rf discharge.[31,43] Liu *et al.*,[7] however, observe increasing maximum ion kinetic energies with increasing applied voltage. This difference may be due to the more symmetric geometry (i.e., equal effective areas of the electrodes) of the rf cell used by Liu and coworkers, as compared to the asymmetric geometry of the GEC cell.

At pressures greater than 13.3 Pa, the time-averaged sheath potential is difficult to determine from IEDs for applied rf voltages below 100 V, because the maximum kinetic energies of the detected ions are substantially reduced by ion-atom collisions. Even the IEDs for Ar_2^+ and ArH^+ ions, that normally exhibit minor collisional effects, are seen to be peaked closer to thermal energy for plasmas with pressures greater than 13.3 Pa (see Fig. 9). As the pressure increases, the IEDs reach an equilibrium where the kinetic energy gained from the electric field is lost through collisions. The shapes of the IEDs eventually become nearly independent of pressure when the ions experience many collisions while crossing the sheath. The IEDs then begin to resemble Maxwellian kinetic-energy distributions indicative of ions that attain an equilibrium condition such as can occur in a uniform-field drift tube[44,45] or a low-current dc discharge.[46]

The variation in magnitude of the apparent flux for each individual ion as a function of gas pressure and applied rf voltage can be determined by integrating the IEDs shown in Figs. 4–9 over kinetic energy. Results of these calculations are shown in Fig. 12, along with calculations of mean ion kinetic energies, $\langle \varepsilon \rangle$. The trends in apparent

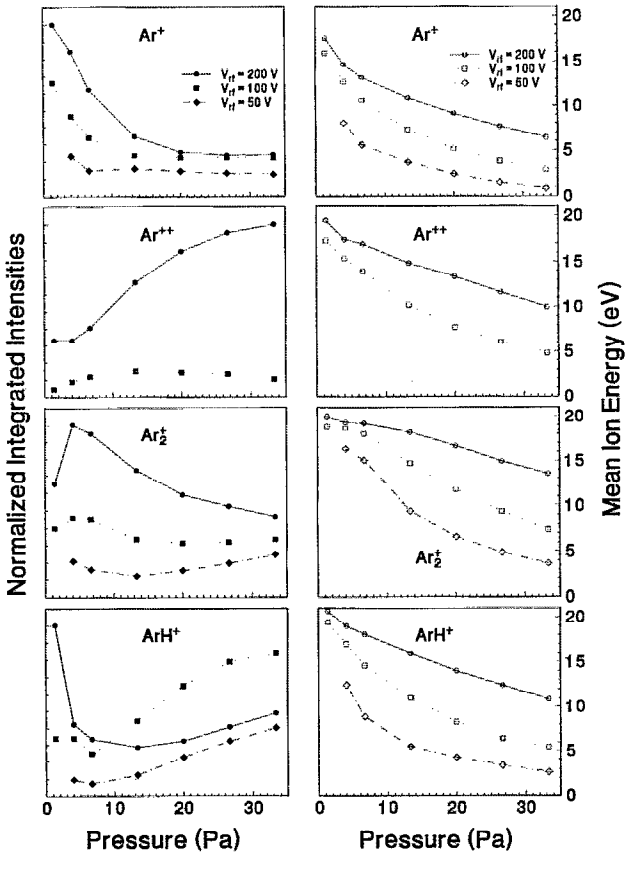

FIG. 12. Integrated intensities and mean energies, $\langle\varepsilon\rangle$, of detected ion flux as a function of gas pressure at the indicated applied voltages. The intensities are calculated by integrating the IEDs presented in Figs. 4–9 over all kinetic energies, and have been normalized to the maximum detected signal for each ion. The mean energies are also calculated from the data presented in Figs. 4–9.

ion flux for each species as a function of gas pressure result from a combination of different factors that include changes in the spatially-dependent ion-production rates, and changes in the mean number of collisions experienced by an ion that could affect the efficiency of its collection.

In the present experiment, an increase in ion discrimination with decreasing energy will give a reduction in the apparent Ar^+ flux as $\langle\varepsilon\rangle$ decreases and a correspondingly greater fraction of the ions have energies below about 5 eV, where discrimination effects are expected to become most significant. This trend is consistent with the results shown in Figs. 4–6, thus suggesting that the measured IEDs could be affected by low-energy ion discrimination. From a comparison of the data in these figures, it can be seen that a decrease of the apparent flux with pressure should be most evident for the highest applied voltage of 200 V. This decrease with pressure is consistent with the data of Seeböch *et al.*,[10] but is inconsistent with observations of Toups and Ernie[8] and by Janes and Huth,[13] who note an increase in Ar^+ flux with increasing pressure for gas pressures ranging from 1–27 Pa.

The integrated intensities for Ar^{++} are observed to increase with increasing pressure, while the mean energy exhibits relatively less drop when compared to Ar^+. The results at 200 V indicate that the observed Ar^{++} flux is primarily determined by an increase in production with pressure, rather than with effects of ion discrimination, such as associated with changes in angular spread due to scattering. Additionally, as the rf voltage changes from 200 V to 100 V, the apparent Ar^{++} flux drops by nearly an order of magnitude. This is expected to be a result of a decrease in the relative number of high-energy electrons present in the discharge that are required for the formation of this ion. The fact that no Ar^{++} signal was detected for $V_{rf}=50$ V is consistent with a drop in the time-averaged sheath potentials, as implied by the reduction in V_1 and V_b (see Table I), below the energy of 27.6 eV required for Ar^{++} formation.

The apparent Ar_2^+ flux also appears to be less affected by discrimination associated with the changes in angular spread due to scattering. This is to be expected since Ar_2^+ is thought to be formed by three-body collisions, which are necessarily pressure dependent, and because Ar_2^+ is less affected by scattering in the sheath. The peaks in detected flux observed in Fig. 12, as well as the general rise in the Ar_2^+ signal with pressure for $V_{rf}=100$ and 50 V, are evidence of the pressure dependent production. Similarly, the relatively minor decreases in $\langle\varepsilon\rangle$ are evidence of fewer significant scattering events that would produce Ar_2^+ with trajectories at large incident angles to the electrode surface. The decrease in apparent Ar_2^+ flux with increasing pressure for $V_{rf}=200$ V suggests occurrence of dissociative ion-molecule collisions in the sheath that destroy Ar_2^+.

The trends in detected ArH^+ current with changing pressure are difficult to interpret since formation of this ion is dependent upon the presence of impurities, and may involve several competing chemical processes that have not been identified.

ACKNOWLEDGMENTS

The authors would like to thank M. A. Sobolewski for his assistance in obtaining the voltage and current data. Partial support for this work was provided by the NIST Foreign Guest Scientist Program. RS acknowledges the financial support received from the S.E.R.C. and Hiden Analytical Ltd. through the "CASE" Awards scheme.

[1] H. F. Winters, J. W. Coburn, and T. J. Chuang, J. Vac. Sci. Technol. B **1**, 469 (1983).
[2] O. Joubert, R. Burke, L. Vallier, C. Martinet, and R. A. B. Devine, Appl. Phys. Lett. **62**, 228 (1993).
[3] K. Köhler, J. W. Coburn, D. E. Horne, E. Kay, and J. H. Keller, J. Appl. Phys. **57**, 59 (1985).
[4] K. Köhler, D. E. Horne, and J. W. Coburn, J. Appl. Phys. **58**, 3350 (1985).
[5] W. M. Greene, M. A. Hartney, W. G. Oldham, and D. W. Hess, J. Appl. Phys. **63**, 1367 (1988).
[6] S. G. Ingram and N. St. J. Braithwaite, J. Phys. D: Appl. Phys. **21**, 1496 (1988).
[7] J. Liu, G. L. Huppert, and H. H. Sawin, J. Appl. Phys. **68**, 3916 (1990).
[8] M. F. Toups and D. W. Ernie, J. Appl. Phys. **68**, 6125 (1990).
[9] C. Wild and P. Koidl, Appl. Phys. Lett. **54**, 505 (1989); J. Appl. Phys. **69**, 2909 (1991).
[10] R. J. Seeböck, W. E. Köhler, and M. Römheld, Contrib. Plasma Phys. **32**, 6 (1992).

[11] A. D. Kuypers and H. J. Hopman, J. Appl. Phys. **63**, 1894 (1988); **67**, 1229 (1990).
[12] A. Manenschijn, G. C. A. M. Janssen, E. van der Drift, and S. Radelaar, J. Appl. Phys. **69**, 1253 (1991).
[13] J. Janes and C. Huth, J. Vac. Sci. Technol. A **10**, 3522 (1992).
[14] M. J. Kushner, J. Appl. Phys. **58**, 4024 (1985).
[15] H. W. Trombley, F. L. Terry, and M. E. Elta, IEEE Trans. Plasma Sci. **19**, 158 (1991).
[16] M. S. Barnes, J. C. Forster, and J. H. Keller, IEEE Trans. Plasma Sci. **19**, 240 (1991).
[17] W. J. Goedheer and P. M. Meijer, IEEE Trans. Plasma Sci. **19**, 245 (1991).
[18] A. Manenschijn and W. J. Goedheer, J. Appl. Phys. **69**, 2923 (1991).
[19] D. Field, D. F. Klemperer, P. W. May, and Y. P. Song, J. Appl. Phys. **70**, 82 (1991).
[20] P. W. May, D. Field, and D. F. Klemperer, J. Appl. Phys. **71**, 3721 (1992).
[21] J. K. Olthoff, R. J. Van Brunt, and S. B. Radovanov, J. Appl. Phys. **72**, 4566 (1992).
[22] P. J. Hargis, K. E. Greenberg, P. A. Miller, J. B. Gerardo, J. R. Torczynski, M. E. Riley, G. A. Hebner, J. R. Roberts, J. K. Olthoff, J. R. Whetstone, R. J. Van Brunt, M. A. Sobolewski, H. A. Anderson, M. P. Splichal, J. L. Mock, P. Bletzinger, A. Garscadden, R. A. Gottscho, G. Selwyn, M. Dalvie, J. E. Heidenreich, J. W. Butterbaugh, M. L. Brake, M. L. Passow, J. Pender, A. Lujan, M. E. Elta, D. B. Graves, H. H. Sawin, M. J. Kushner, J. T. Verdeyen, R. Horwath, and T. R. Turner, Rev. Sci. Instrum. (in press).
[23] J. K. Olthoff, R. J. Van Brunt, S. B. Radovanov, and J. A. Rees, IEE Proc. A (in press).
[24] M. A. Sobolewski, J. Vac. Sci. Technol. A **10**, 3550 (1992).
[25] J. R. Roberts, J. K. Olthoff, R. J. Van Brunt, and J. R. Whetstone, *Advanced Techniques for Integrated Circuit Processing* (Society of Photo-Optical Instrumentation Engineers, Bellingham, WA, 1991), Vol. 1392, pp. 428–436.
[26] Certain commercial equipment, instruments, or materials are identified in this paper to specify adequately the experimental procedure. Such identification does not imply recommendation or endorsement by the National Institute of Standards and Technology, nor does it imply that the materials or equipment identified are necessarily the best available for the purpose.
[27] P. A. Miller, H. Anderson, and M. P. Splichal, J. Appl. Phys. **71**, 1171 (1992).
[28] J. W. Coburn and E. Kay, J. Vac. Sci. Technol. **8**, 738 (1971).
[29] D. A. Dahl, J. E. Delmore, and A. D. Appelhans, Rev. Sci. Instrum. **61**, 607 (1990).
[30] R. Surowiec and J. A. Rees (unpublished).
[31] J. P. Beouf and Ph. Belenguer, in *Nonequilibrium Processes in Partially Ionized Gases*, edited by M. Capitelli and J. N. Bardsley (Plenum, New York, 1990), p. 155.
[32] R. Johnsen, A. Chen, and M. A. Biondi, J. Chem. Phys. **73**, 1717 (1980).
[33] M. Grossl, M. Langeirwalter, H. Helm, and T. D. Mark, J. Chem. Phys. **74**, 1728 (1981).
[34] A. V. Phelps, J. Phys. Chem. Ref. Data **20**, 557 (1991).
[35] A. V. Phelps, J. Phys. Chem. Ref. Data **21**, 883 (1992).
[36] M. J. Vasile and H. F. Dylla, in *Plasma Diagnostics*, edited by O. Auciella and D. L. Flamm (Academic, New York, 1989), Vol 1, pp. 185–237.
[37] N. Mutsukura and G. Turban, Plasma Chem. Plasma Proc. **10**, 27 (1990).
[38] J. K. Olthoff, R. J. Van Brunt, and M. A. Sobolewski, *Proceedings of the Tenth International Conference on Gas Discharges and their Applications* (Swansea, Wales, 1992), pp. 440–443.
[39] M. A. Sobolewski and J. K. Olthoff, *Microelectronic Processes, Sensors and Controls for Micro* (Society for Photo-Optical Instrumentation Engineers, Bellingham, WA, in press), Vol. 2091.
[40] E. W. McDaniel, V. Cěrmák, A. Dalgarno, E. E. Ferguson, and L. Friedman, *Ion-Molecule Reactions* (Wiley-Interscience, New York, 1970).
[41] M. A. Sobolewski and J. R. Whetstone, *Advanced Techniques for Integrated Circuit Processing II* (Society for Photo-Optical Instrumentation Engineers, Bellingham, WA, 1993), Vol. 1803, pp. 309–320.
[42] S. Djurović, J. R. Roberts, M. A. Sobolewski, and J. K. Olthoff, J. Res. Natl. Inst. Stand. Technol. **98**, 159 (1993).
[43] P. W. May, D. F. Klemperer, and D. Field, J. Appl. Phys. **73**, 1634 (1993).
[44] T. Makabe and H. Shinada, J. Phys. D: Appl. Phys. **18**, 2385 (1985).
[45] P. P. Ong and M. J. Hogan, J. Phys. D: Appl. Phys. **18**, 1897 (1985).
[46] S. B. Vrhovac, B. M. Jelenkovic, J. K. Olthoff, and R. J. Van Brunt, *Proceedings of the Tenth International Conference on Gas Discharges and their Applications* (Swansea, Wales, 1992), pp. 510–512.